Linear conversion of pressure into concentration, rapid switching of concentration, and generation of linear ramps of concentration in a microfluidic device

Micha Adler and Alex Groisman[a)]
Department of Physics, University of California, San Diego, 9500 Gilman Drive, MC 0374, La Jolla, California 92093, USA

(Received 4 August 2011; accepted 22 January 2012; published online 13 April 2012)

Mixing of liquids to produce solutions with different concentrations is one of the basic functionalities of microfluidic devices. Generation of specific temporal patterns of concentration in microfluidic devices is an important technique to study responses of cells and model organisms to variations in the chemical composition of their environment. Here, we present a simple microfluidic network that linearly converts pressure at an inlet into concentration of a soluble reagent in an observation region and also enables independent concurrent linear control of concentrations of two reagents. The microfluidic device has an integrated mixer channel with chaotic three-dimensional flow that facilitates rapid switching of concentrations in a continuous range. A simple pneumatic setup generating linear ramps of pressure is used to produce smooth linear ramps and triangular waves of concentration with different slopes. The use of chaotic vs. laminar mixers is discussed in the context of microfluidic devices providing rapid switching and generating temporal waves of concentration. © *2012 American Institute of Physics*. [doi:10.1063/1.3687379]

I. INTRODUCTION

Generation of a solution with a desired concentration, C, out of a stock solution with a high concentration, C^0, and solvent (or buffer) is one of the basic functions of microfluidic devices. The small diameter of microfluidic channels typically leads to relatively rapid equilibration of concentrations (mixing) across the channels. Mixing can also be greatly accelerated by generation of 3-dimensional (3D) flow with a microfluidic mixer.[1,2] Therefore, a desired solution can, in principle, be readily prepared in a microfluidic device by combining a concentrated solution and solvent in appropriate proportions. Nevertheless, accurate control of the proportions can present a practical problem. In a continuous flow system with controlled volumetric fluxes of concentrated solution, Q_1, and solvent, Q_2, the resulting concentration can be evaluated as $C = C^0 Q_1/(Q_1 + Q_2)$ and is thus a non-linear function of both Q_1 and Q_2, when C is an appreciable fraction of C^0. Moreover, changing one volumetric flux at a time leads to variation of the flow velocity and substrate shear stress that may be undesirable. In addition, syringe and peristaltic pumps, which are commonly used to control volumetric fluxes, often operate unevenly, thus leading to substantial fluctuations of C, and do not allow rapid switching of concentration.

Small volumes of liquid can be accurately metered with integrated membrane valves,[3] making it possible to mix liquids in well-defined proportions and generate solutions with precisely controlled concentrations.[3,4] However, microfluidic devices with membrane valves have relatively complicated two-layer construction. In addition, the adjustment of concentration is discrete rather than continuous, has a relatively long switching time, and involves variations of

[a)]Author to whom correspondence should be addressed. Electronic mail: agroisman@ucsd.edu. Tel.: 858-822-1838.

flow velocity. Rapid concentration switching and low fluctuations are both achievable in pressure-driven flows. Nevertheless, the linear conversion of pressure into concentration and variation of concentration without concomitant variation of flow velocity still remain problematic, and simultaneous variation of multiple concentrations presents an even bigger challenge.

Problems closely related to the generation of a solution with a desired concentration are the production of spatial gradients and temporal patterns (waves) of concentration. Spatial gradients of concentration can be produced by mixing liquids fed into the microfluidic device in different proportions and letting streams of the resulting solutions with different concentrations flow side-by-side to create a smooth spatial profile.[5,6] While the main application of microfluidic gradients has been studies of chemotaxis,[7] this technique has also been used to obtain a desired concentration in a designated microchannel for the purposes of titration,[8] studies of cell dose response,[9–11] and variation of refractive index of the medium.[12]

As has been shown in classic experiments on *Escherichia coli* chemotaxis,[13–15] exposure of cells to specific temporal patterns (waves) of concentration of a stimulus is a powerful technique for studying chemotaxis and the dynamics of cellular responses, adaptation, and signal processing. Temporal variations of stimulus concentration generated in microfluidic devices have been applied to study the dynamics of gene expression of various cells[16–20] and responses of budding yeast (*Sacchromyces cereviciae*) to osmotic shock.[21,22] It is worth noting, however, that whereas the time scales of changes in gene expression and of response to osmotic shock are $\sim$1 h and $\sim$1 min, respectively, responses of chemotactic bacterial[13–15] as well as eukaryotic cells[23–26] to changes in concentration of chemoattractant can occur on a timescale of 1 s. Therefore, studies of responses and signaling of chemotactic cells (as well as some other non-transcriptional responses[27,28]) require particularly high time resolution and accurate definition of temporal patterns of stimuli presented to cells.

Before the introduction of modern microfluidic technologies, temporal waves of concentrations were generated by rapid discharge of a concentrated solution from micropipettes,[13,15] alternative injection of solutions with different concentrations,[23] and by controlling volumetric fluxes with syringe pumps.[14,24] Injection of solutions with different concentrations has also been used to generate binary temporal patterns of concentration in microfluidic devices,[16,18,22,28,29] with the switching times as short as $\sim$0.1 s.[30] Another specifically microfluidic technique for generation of (mostly binary) temporal patterns of concentration in a given area has relied on lateral shifting of the interface between streams of solutions with different concentrations.[19,21,31,32] Various periodic waves of concentrations have been generated in pressure-driven flows, with electronic pressure controllers producing specific temporal patterns of pressure.[17,33] Pressure actuated membrane valves have been used to create complex patterns of concentration of multiple substances[34] and, in combination with consecutive dilution channel networks, to switch between a set concentrations, generating desired concentrations bit-by-bit and generating temporal waves.[35] Membrane valves have also been used to switch the feeding of a mixing channel between a concentrated solution and solvent, setting proportions of the two liquids and generating waves of concentrations by controlling and varying the duty cycle.[36,37] In addition, temporal waves of concentration have been generated by dynamically controlling the duty cycles of on-chip micropumps based on membrane valves.[38,39] Control of the duty cycle of multiple pumps also enabled independent adjustment and generation of temporal waves of concentration of multiple analytes.[39] Out of these microfluidic techniques, continuous ranges of concentration were provided by the dynamic control of driving pressure[17,33] and of duty cycles.[36–38] However, in the former case, control of concentration required concurrent variation of two pressures and the frequency was limited to 0.2 Hz (Ref. 19) (or less[35]), whereas in the latter case, the devices had complex, multi-layer constructions, and accessible frequencies were even lower.

Here, we describe a simple single-layer microfluidic network enabling linear conversion of pressure at an inlet into concentration of a substance in an observation area, C, in the entire range from zero to the concentration of the stock solution fed to this inlet, C^0, without changes in flow velocity in the observation area. The microfluidic network also makes it possible to independently vary concentrations of two substances by adjusting pressures at two inlets, with a

linear relation between the pressures and respective concentrations and without any cross-talk. The microfluidic network has an integrated mixer with a steady three-dimensional flow that is chaotic in the Lagrangian sense, whose design has been optimized to enable switching the concentrations in the observation area within 0.25 s (based on a 10% to 90% criterion), while keeping the flow rate at a constant high value. A simple setup consisting of a large-volume reservoir and a long narrow capillary, an analogue of an electronic *RC*-circuit, is used to generate linear ramps of inlet pressure, producing particularly smooth, prolonged linear ramps of concentration with various positive and negative slopes, as well as various triangular (and saw tooth) waves of concentration. Finally, the switching time of laminar microfluidic mixers and the use of chaotic vs. laminar mixers for applications requiring rapid switching of concentration are discussed.

II. EXPERIMENTAL

A. The flow-driving setup and architecture of the microfluidic device

The microfluidic device [Fig. 1(a)] has a single outlet and three inlets, the buffer inlet, for plain buffer, and the inlets 1 and 2 for stock solutions of two different reagents. The flow in the device is driven by the application of differential pressures between each of the three inlets and the outlet, P_{buf}, P_1, and P_2, respectively. Volumetric fluxes, Q, in channels of the device depend on the differential pressures, ΔP, applied across the channels and hydrodynamic

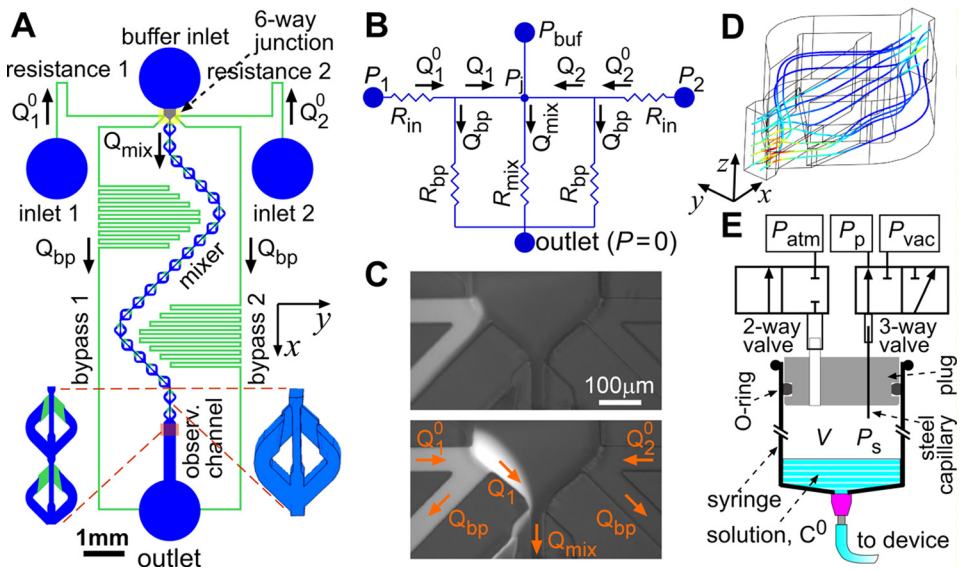

FIG. 1. Microfluidic device and pressure ramp generating setup. (a) Layout of the microfluidic device. 50 and 180 μm deep channels are shown in green and blue, respectively. Arrows indicate direction of flow. The region of the observation channel, where concentrations are tested, is highlighted in red. *Insets*: 4× magnified drawing of two consecutive segments of the mixer channel (left) and three-dimensional drawing of a segment (right). (b) Microfluidic network represented as a schematic wire diagram, showing volumetric fluxes through various channels and junctions (arrows and Q-labels), hydrodynamic resistances of various channels (resistance symbols and *R*-labels), and pressures, *P*, at various points (inlets, outlet, and 6-way junction). (c) Micrographs of a region of the 6-way junction [highlighted in yellow in (a)] taken under mixed fluorescence/brightfield illumination. The center top of each micrograph is the lower edge of the buffer inlet and the center bottom is the entrance to the mixer channel. *Top*: $P_{buf} < P_1 < P_{th}$ and fluorescein solution with $C_1^0 = 4$ ppm fed to inlet 1 that arrives at the 6-way junction is entirely diverted into bypass channel 1 and does not reach the mixer channel, resulting in $C_1 = 0$. *Bottom*: $P_{th} < P_1 < P_{over}$ and a part of fluorescein solution that arrives at the 6-way junction enters the mixer channel, resulting in $0 < Q_1 < Q_{mix}$ and $0 < C_1 < C_1^0$. (d) Results of a numerical simulation of flow in a segment of the mixer using Comsol. Flow is shown by color-coded streamlines, with red corresponding to highest and blue to lowest speed, respectively. (e) A setup based on a 140 cc syringe (analogue of a capacitor) and thin capillary (fluidic resistor), comprising a pneumatic *RC*-circuit for generation of linear time ramps of pressure of the solution held in the syringe. The 3-way valve alternatively connects the syringe to pressurized air or vacuum through the capillary, and the 2-way valve alternatively seals the syringe or vents it to atmosphere.

resistances of the channels, R, which are defined as $R = \Delta P/Q$. (The relation between ΔP and Q is linear, because the device operates in the laminar flow regime.) The solutions fed to the inlets and drawn out from the outlet are held in modified 140 cc plastic syringes that are connected to the device through polyvinyl chloride (PVC) tubing lines and short segments of hypodermic tubing. The syringes are attached to stages sliding along vertical rails with a high-resolution rules attached to the rails, making it possible to adjust pressure at the inlets hydrostatically with an accuracy of $\sim$2 Pa by setting the level of liquid in the syringes.[40] In addition, the syringes connected to the inlets 1 and 2 can be pressurized by compressed air.

The device has channels of two different depths, 50 and 180 μm, and consists of three main elements: resistor channels, a mixer channel, and an observation channel [Fig. 1(a)]. The resistor channels are all 50 μm deep, the mixer channel is comprised of 50 and 180 μm deep elements as explained below, whereas the observation channel is 180 μm deep. The mixer channel is fed with plain buffer coming from the buffer inlet and with two stock solutions coming from the inlets 1 and 2 and containing substances 1 and 2 at concentrations C_1^0 and C_2^0, respectively. The mixer serves the purpose of delivering to the observation channel a thoroughly mixed solution with reduced concentrations of the two substances, C_1 and C_2. The resistor channels form four separate lines [Fig. 1(a)]: resistors 1 and 2, connecting the inlets 1 and 2 with the mixer entrance, that have identical resistances R_{in} and bypass channels 1 and 2 that also have identical resistances, R_{bp}, and connect the mixer entrance with the outlet on the sides of inlets 1 and 2 [see equivalent circuit in Fig. 1(b)]. The bypass channels as well as the channels connecting the three device inlets with the mixer entrance all join in a small area, forming a 6-way junction [Fig. 1(c)].

The resistor channels of the device are designed to make C_1 and C_2 linear functions of P_1 and P_2, respectively. To this end, the resistance of the channel connecting the buffer inlet with the mixer entrance is made negligibly small compared with the other channel resistances (R_{in}, R_{bp}, and R_{mix}; see below) by making this channel short, wide, and deep. In addition, the tubing line connecting the buffer inlet with the buffer reservoir has a large diameter (1/16 in.) and thus a minimal hydrodynamic resistance. As a result, the differential pressure between the six-way junction (mixer entrance) and the outlet, P_j, is expected to be practically indistinguishable from the differential pressure between the buffer reservoir and the outlet, P_{buf}, and independent of either P_1 or P_2. Therefore, the volumetric flux through the mixer channel, $Q_{mix} = P_j/R_{mix}$ is practically equal to P_{buf}/R_{mix} and is thus solely defined by P_{buf} and independent of either P_1 or P_2. (Here, R_{mix} is the combined hydrodynamic resistance of the mixer and observation channel). Here and in what follows, we assume that solutions fed to all three inlets have identical viscosities and densities, which is a reasonable assumption for biological experiments, in which concentrations of active ingredients (C_1^0 and C_2^0) are usually low.

Because the resistor channels 1 and 2 are connected to the respective bypass channels somewhat upstream of the mixer entrance [Fig. 1(c)], in the equivalent circuit in Fig. 1(b), the six-way junction is represented by a combination of a four-way junction and two T-junctions on its sides. Because of the proximity between the resistor 1, 2 and bypass channel 1, 2 connection points and the mixer channel entrance [Figs. 1(a) and 1(c)], the corresponding hydrodynamic resistances are negligible, similar to the resistance of the channel connecting the buffer inlet with the mixer entrance. Therefore, these connections are represented by simple wires in the circuit in Fig. 1(b) and the pressures at both T-junctions are practically equal to P_{buf} as well. Hence, the volumetric fluxes through the bypass channels, Q_{bp}, are equal to each other, both given by $Q_{bp} = P_{buf}/R_{bp}$, and, just as Q_{mix}, independent of either P_1 or P_2.

The parameters controlled by P_1 and P_2 are the volumetric fluxes through the respective inlets, $Q_1^0 = (P_1 - P_j)/R_{in} = (P_1 - P_{buf})/R_{in}$ and $Q_2^0 = (P_2 - P_{buf})/R_{in}$. The device is operated in a regime with $P_1 > P_{buf}$ and $P_2 > P_{buf}$, so both Q_1^0 and Q_2^0 are positive, corresponding to flow directed from the inlets towards the respective T-junctions. (Alternatively, one of the inlets may be blocked). Nevertheless, as long as $Q_1^0 < Q_{bp}$, corresponding to $(P_1 - P_{buf})/R_{in} < P_{buf}/R_{bp}$ and $P_1 < P_{buf} + P_{buf}R_{in}/R_{bp}$, the entire flux from inlet 1 is diverted to the bypass channel 1 and does not reach the mixer channel. Therefore, as long as P_1 is below a threshold level, $P_{th} = P_{buf} + P_{buf}R_{in}/R_{bp}$, the value of C_1 is exactly zero. By the same token, C_2 in the observation

channel remains zero for $P_2 < P_{th}$. However, once P_1 exceeds this threshold level ($P_1 > P_{th}$), there is a flow of solution 1 towards the four-way junction and through the mixer channel at a volumetric flux $Q_1 = Q_1^0 - Q_{bp} = (P_1 - P_{th})/R_{in}$. [When $Q_1^0 < Q_{bp}$, in terms of the equivalent circuit in Fig. 1(b), the flux Q_1 is negative.] The flux Q_1 is proportional to the level of P_1 above the threshold, $\Delta P_1 = P_1 - P_{th}$, because the flux through the bypass channel, Q_{bp}, is independent of P_1 and remains unchanged. Moreover, because the total flux through the mixer channel does not depend on variations of P_1 either (it is $Q_{mix} = P_{buf}/R_{mix}$), the part of the flux of solution 1 in the total flux through the mixer is $\frac{Q_1}{Q_{mix}} = \frac{\Delta P_1}{Q_{mix}R_{in}}$ and is a linear function of ΔP_1 as well. (The flux of solution 1 through the mixer grows with P_1 at the expense of the flux of the buffer that linearly decreases with P_1 as $Q_{mix} - Q_1 = \frac{P_{buf}}{R_{mix}} - \frac{\Delta P_1}{R_{in}}$.) After the solution from inlet 1 is mixed with the buffer, the ratio between the concentration of substance 1 in the observation channel and its concentration in the stock solution, C_1/C_1^0, becomes the same as the flux ratio, $\frac{C_1}{C_1^0} = \frac{Q_1}{Q_{mix}} = \frac{\Delta P_1}{Q_{mix}R_{in}}$, so $C_1 = C_1^0 \frac{\Delta P_1}{Q_{mix}R_{in}}$. Therefore, just as Q_1, C_1 is also a linear function of ΔP_1 and P_1.

This linear dependence is only violated when $Q_1 > Q_{mix}$. In this case, the entire liquid entering the mixing channel comes from inlet 1, resulting in $C_1 = C_1^0$. The value of P_1, at which this overflow occurs, P_{over}, is found from the condition $Q_1 = Q_{mix}$, giving $P_{over} = P_{th} + Q_{mix}R_{in} = P_{th} + P_{buf}R_{in}/R_{mix}$. The operation of the device at $P_1 > P_{over}$ can result in flow of the solution of substance 1 towards the buffer inlet and is generally to be avoided. However, if inlet 2 is blocked, Q_1 can exceed Q_{mix} by as much as Q_{bp}, without causing the buffer flow inversion. This fact can be used to experimentally find P_{over} as the value of P_1 at which the solution of substance 1 starts penetrating into bypass channel 2 and the growth of C_1 with P_1 in the observation channel is saturated. Once P_{th} and P_{over} are experimentally determined, C_1 can be found as $C_1 = C_1^0 \frac{P_1 - P_{th}}{P_{over} - P_{th}}$, providing a straightforward practical way to calculate the value of P_1 required to obtain a desired concentration, C_1, $P_1 = P_{th} + (P_{over} - P_{th})\frac{C_1}{C_1^0}$.

The analysis in the previous paragraphs can be equally applied to the flow from inlet 2, leading to a conclusion that the concentration of substance 2 in the observation channel should be $C_2 = C_2^0 \frac{P_2 - P_{th}}{P_{over} - P_{th}}$, where P_{th} and P_{over} are the same as before. (Both of these parameters are independent of either P_1 or P_2.) Nevertheless, when the inlets 1 and 2 are both contributing flux to the mixer, an obvious restriction applies that the sum of the fluxes of solutions 1 and 2 through the mixer, $Q_1 + Q_2$, is smaller than the total flux through the mixer, Q_{mix}, corresponding to $\frac{C_1}{C_1^0} + \frac{C_2}{C_2^0} \leq 1$. Indeed, the device does not function properly if $Q_1 + Q_2 > Q_{mix}$, due to inversion of the buffer flow.

The above analysis of the device operation can be reduced to three major statements. (1) When solutions of substances 1 and 2 with concentrations C_1^0 and C_2^0, respectively, are fed to the inlets 1 and 2, the concentrations of the two substances in the observation channel, C_1 and C_2, are linear functions of pressures at the corresponding inlets, P_1 and P_2, as long as P_1 and P_2 are in the range between P_{th} and P_{over}. If P_1 or P_2 is lower than P_{th}, the concentration of the corresponding substance in the observation channel is zero. (2) The conversion of pressures P_1 and P_2 into respective concentrations C_1 and C_2 has a simple form $C_i = C_i^0 \frac{P_i - P_{th}}{P_{over} - P_{th}} = C_i^0 \frac{\Delta P_i}{P_{over} - P_{th}}$, with the constants P_{th} and P_{over} identified experimentally as the values of P_1 (or P_2) at which substance 1 (or 2) first appears in the observation channel and at which it penetrates to bypass channel 2 (or 1), respectively. (3) The concentrations C_1 and C_2 are individually controlled by the pressures P_1 and P_2, respectively, without any dependence of C_1 on P_2 or C_2 on P_1 other than in the case of the overflow (buffer flow inversion).

Hydrodynamic resistances in the device were chosen such that the flow could be driven by both hydrostatic pressure and pressure of compressed air. Specifically, the value of R_{mix} was such that at a driving pressure $P_{buf} = 5.0$ kPa (~50 cm of water column) the flow rate through the mixer channel was high (0.27 μl/s) and mixing was practically complete (Sec. III B). The resistance ratios were $R_{in}/R_{mix} \approx 1.8$ and $R_{bp}/R_{mix} \approx 23$, resulting in the key pressure differences $P_{th} - P_{buf}$ and $P_{over} - P_{th}$ with values of 0.4 and 9.1 kPa, respectively. The former pressure difference was large enough to use hydrostatic pressure to conveniently set P_1 (and P_2) between P_{buf} and P_{th} that resulted in $C_1 = 0$ (and $C_2 = 0$), while providing positive flow through inlet 1

(and 2) towards the bypass channel. So, once P_1 was raised to a level between P_{th} and P_{over}, C_1 would follow with a minimal delay. The difference $P_{over} - P_{th}$ was small enough to enable the adjustment of C_1 and C_2 with hydrostatic pressure, resulting in high precision and temporal stability, and also large enough to minimize the effect of mechanical vibrations and to allow rapid switching of C_1 (and C_2) by connecting inlet 1 (and 2) to compressed air through a solenoid valve.

B. Mixer channel

The mixer channel of the device [Fig. 1(a)] is a modification of the microfluidic mixer from a previous publication[2] and consists of a chain of 22 mirror-symmetric segments with 50 and 180 μm deep elements, generating three-dimensional (3D) flow with stretching and folding that promotes efficient mixing [Fig. 1(d) and insets in Fig. 1(a)]. (Some parts of the mixer chain are tilted at 45° to reduce the device footprint.) Briefly, at the entrance of each segment, the stream is split three-ways, forward towards a tall and narrow (180 μm deep and 30 μm wide) central channel and to two shallow (50 μm deep) side channels on the bottom left and bottom right, resulting in stretching of the stream in the direction out of plane of the device [z-direction; Fig. 1(d)]. At the end of the segment, the three streams merge into one, resulting in folding. The mixer channel of the device has elements with the same depth as in the microfluidic mixer in Ref. 2, but is different from it in several respects. First, the segments are mirror-symmetric rather than identical [Fig. 1(a)], and different geometries of the side branches lead to different flow resistances. As a result, according to numerical simulations of the flow using Comsol, the volumetric flow rates through the side branches differ ~2-fold, leading to uneven splitting of the flow [43%, 34%, and 23% for the right, central, and left branches for the segment shown in Fig. 1(d)]. This uneven splitting and the alteration of the segments with larger flow to the right and to the left branches are designed to make the mixing more chaotic (in the Lagrangian sense) and, by breaking the right/left symmetry, to prevent the undesirable situation when the solution coming from inlet 1 (or 2) mostly remains on the left (right) side of the mixer.

Second, the design of the mixer segments is optimized through numerical simulations in Comsol to reduce the passage time of the solution through them (residence time) and the variation of passage time along different streamlines (variation of residence time), without compromising the efficiency of mixing or making their flow resistance excessively high. The mean passage time through the mixer defines the delay between changes of the inlet pressures (P_1 and P_2) and of the concentrations in the observation channel (C_1 and C_2). No less important, the passage time is one of the factors defining the concentration switching time, which is the duration of transition from the old to the new levels of C_1 (or C_2) after P_1 (or P_2) is abruptly switched. For example, for a laminar mixer (straight channel with rectilinear flow), the switching time is proportional to a square root of the passage time (see Eq. (5) in Sec. IV B). The main factor defining the switching time is the variation of the passage time between different flow trajectories (dispersion), and for generation of both abrupt steps and well-defined temporal waves of concentration, it is desirable to have the variation of the mean passage time as small as possible.

The mean passage time at a given volumetric flux is inversely proportional to the total volume of channels in the mixer. Therefore, the channels in the segments of the present mixer were made substantially shorter and narrower than in Ref. 2, resulting in ~10-fold reduction of the volume of a segment, from ~100 nl to ~10 nl [cf. Fig. 1(d) and insets in Fig. 1(a) vs. Fig. 1 from Ref. 2]. To reduce the variation of the passage time, the 180 μm deep channels in the mixing segments were streamlined by introducing smooth round turns instead of corners present in the design in Ref. 2, thus eliminating regions with particularly slow flow (where the liquid can stay for a prolonged time). In addition, an effort was made to reduce differences between the mean passage times (volumetric fluxes divided by volumes) through the central and side branches of a segment, given other requirements of the design and constraints of the microfabrication.

C. Generation of linear ramps of concentration

To use the linear relationship between the inlet pressures, P_1 and P_2, and the respective solution concentrations, C_1 and C_2, in order to produce linear time ramps of concentration, we needed to generate linear time ramps of pressure. To this end, we inserted an O-ring sealed plug into a 140 cc plastic syringe, inserted a long and thin steel capillary (40 mm length, 50 μm effective internal diameter) into a through-hole in the plug, and connected the distal end of capillary to a common port of a 3-way solenoid valve (P251SS-O12 by Ingersoll Rand), with its two other ports connected to sources of pressurized air and vacuum [Fig. 1(e)]. The plug had another opening, connecting the interior of the syringe to atmosphere through a normally closed 2-way solenoid valve [Fig. 1(e)].

Actuation of the 2-way valve rapidly vents the syringe, equilibrating the pressure in the syringe with the atmospheric pressure. (We note that in the following discussion of the pneumatic setup, all pressure values are absolute rather than gauge pressures.) When the 2-way valve is closed and the distal end of the capillary is connected to a source of pressurized air with pressure P_p, air flows into the syringe at a volumetric flux $Q_s = (P_p - P_s)/R_c$, where P_s is the pressure inside the syringe and R_c is the hydrodynamic resistance of the capillary. This flow of air causes the pressure inside the syringe to increase at a rate $dP_s/dt = Q_s P_s/V$, where V is the volume of air in the syringe. This system is similar to an electronic RC-circuit, with the roles of the resistance and capacitance (R and C) played by R_c and V, respectively. In the first approximation (the fractional change in P_s being small, which is true as long as P_s remains close to the atmospheric pressure), P_s varies like the voltage of a charging capacitor, $P_s(t) = (P_p - P_s^0)[1 - \exp(-t/\tau)] + P_s^0$, where $\tau = R_c V/P_s^0$ and P_s^0 is the initial pressure in the syringe. Furthermore, at times $t \ll \tau$, $P_p - P_s$ is nearly equal to $P_p - P_s^0$ and Q_s remains nearly constant, leading to a practically linear increase in the pressure inside the syringe at a rate $dP_s/dt = (P_p - P_s^0)/\tau$. Therefore, if one chooses a capillary with sufficiently large hydrodynamic resistance, R_c, to obtain a large value of τ, one can achieve practically linear ramp of pressure in the syringe over an extended period of time. (The choice of the syringe volume at a relatively high value of 140 cc was also intended to achieve large τ.) Most importantly, the proposed setup does not have any moving mechanical parts, relying instead on a simple pneumatic process, and can thus provide practically smooth ramps of pressure, P_s.

We further note that the above reasoning also applies in the case, when the distal end of the capillary is connected to a source of vacuum [negative gauge pressure; P_{vac} in Fig. 1(e)], resulting in a flow of air out of the syringe and a linear reduction of P_s with time at $t \ll \tau$. We also note that a practical recipe to have the rate of pressure change nearly constant is by keeping $P_s - P_s^0 \ll P_p - P_s^0$, which is limiting variations of pressure in the syringe to a small fraction of $P_p - P_s^0$.

Finally, the above equations need to be amended by accounting for variation of the volumetric flux along the capillary due to the compressibility of air and conservation of mass. Specifically, the flux Q_s is evaluated at the pressure inside the syringe, P_s, which in our experiments was always close to the atmospheric pressure, P_{atm}, whereas the pressure P_p was usually well above or well below P_{atm}. The volumetric flux at the distal end of the capillary, Q_p, can be calculated as $Q_p = Q_s P_s/P_p \approx Q_s P_{atm}/P_p$, assuming an isothermal process. Similarly, the local volumetric flux, Q, along the capillary varies with the local pressure, P, as $Q = Q_s P_s/P$. Because the viscosity of air is nearly pressure independent, for laminar flow in the capillary, the local pressure gradient along the capillary, dP/dx, is given by $dP/dx = kQ = kQ_s P_s/P$ (where k is a coefficient of resistance of the capillary), leading to non-linear distribution of P along the capillary. Integration of this differential equation with the boundary conditions of P_s and P_p at the two ends of the capillary gives $Q_s = (P_p^2 - P_s^2)/(2P_s R_c)$, suggesting a non-linear dependence of Q_s and dP_s/dt on P_p that for $P_s \approx P_{atm}$ becomes $dP_s/dt \approx (P_p^2 - P_{atm}^2)/(2R_c V)$. Nevertheless, this non-linearity does not change the fact that the rate of syringe pressure growth, dP_s/dt, is nearly constant as long as $t \ll \tau$ and $P_s - P_s^0 \ll P_p - P_s^0$.

III. RESULTS

A. Characterization of flow

The device was tested with *p*H 7.5, 10 mM phosphate buffer fed to the buffer inlet and to inlet 2 and a solution of fluorescein sodium salt (called fluorescein in what follows) in this buffer fed to inlet 1. In some experiments, inlet 2 was blocked. The device was operated at a buffer inlet pressure $P_{buf} = 5.0\,\text{kPa}$, which was set hydrostatically. The flow velocity in the 300×180 μm observation channel was measured by tracking 2 μm green fluorescent beads added to the buffer and had a maximal value of $\sim$10 mm/s, corresponding to a mean flow velocity of $\sim$5 mm/s and a volumetric flux $Q_{mix} = 0.27\,\mu\text{l/s}$ (as calculated using laminar flow equations for rectangular channels[41]). With a 10 ppm fluorescein solution fed to inlet 1 and inlet 2 blocked, we varied the pressure at inlet 1, P_1, to observe the thresholds for penetration of fluorescein into the mixer channel and into bypass channel 2 and established the values of P_1 at the two thresholds at $P_{th} = 5.4$ and $P_{over} = 14.5\,\text{kPa}$, respectively.

B. Quality of mixing

We then set P_1 at $\sim$12 kPa and tested the quality of mixing in the mixer channel by taking a stack of fluorescence micrographs of the observation channel [region highlighted in red in Fig. 1(a)] with a spinning-disk confocal microscope. The objective lens was Zeiss $20\times/0.8$ and the step in the *z*-direction was 1 μm. The stack of confocal micrographs was used to reconstruct the distribution of fluorescence in the *yz*-cross-section of the channel (the plane perpendicular to the flow, Fig. 1; see also Ref. 2). The background was evaluated by taking a stack of confocal micrographs of the polydimethylsiloxane (PDMS) chip and subtracted from the *yz*-profile of fluorescence in the channel, resulting in a background-corrected fluorescence profile in Fig. 2(a). The experiment was repeated with the buffer inlet blocked to measure the distribution of fluorescence with homogeneous 10 ppm fluorescein solution [Fig. 2(b)]. The *yz*-profile of fluorescence in the observation channel in Fig. 2(a) does not have any apparent features that may result from incomplete mixing (cf. Fig. 2 in Ref. 2) and is generally uniform apart from some long-range variations that are also seen in Fig. 2(b) (likely due to uneven illumination and light collection), sharp changes in near-wall regions, and some vertical and horizontal lines, which are likely instrumental artifacts. These features are apparent in the *y*-axis profiles of fluorescence taken near the channel mid-planes [Fig. 2(c)]. However, the *y*-axis profiles for the channel cross-sections in Figs. 2(a) and 2(b) are nearly indistinguishable, apart from $\sim$25% lower mean fluorescence for the cross-section in Fig. 2(a) [red vs. blue curve in Fig. 2(c)].

In a central region of the channel cross-section, spanning 70% of its width and height (210×128 μm in the *yz*-plane), the mean pixel values, and standard deviations (SDs) were, respectively, 152 and 9.9 for Fig. 2(a) and 199 and 12.4 for Fig. 2(b). The values of SD were reduced to 3.5 and 5, respectively, for regions spanning 30% of both width and height near the center, corresponding to a coefficient of variations of $\sim$2.5% for profiles in both Figs. 2(a) and 2(b). These results indicate that the variation of pixel values in Fig. 2(a) primarily originates from instrumental noise and long-range non-uniformity of illumination and light collection. Therefore, within the resolution of the imaging system, the 10 ppm solution and buffer were completely mixed after passing through the mixing channel.

C. Linearity of conversion of pressure into concentration

We tested the linearity of the conversion of pressure into concentration, as suggested by the equation $C_1 = C_1^0 \frac{P_1 - P_{th}}{P_{over} - P_{th}}$ above, by measuring the level of fluorescence in the observation channel as a function of inlet pressure, P_1, at $P_{buf} = 5.0\,\text{kPa}$ and with inlet 2 blocked. The experiments were performed on a video-microscopy setup, consisting of an inverted fluorescence microscope (Nikon TE2000) with a FITC filter cube and a $20\times/0.45$ objective and a 12-bit cooled digital camera (Spot-RT6 by Diagnostic Instruments). The source of fluorescence illumination was a high-power air-cooled light emitting diode (LED) with a center wavelength of 455 nm. The LED was driven by a stabilized DC power supply, resulting in the fluorescence

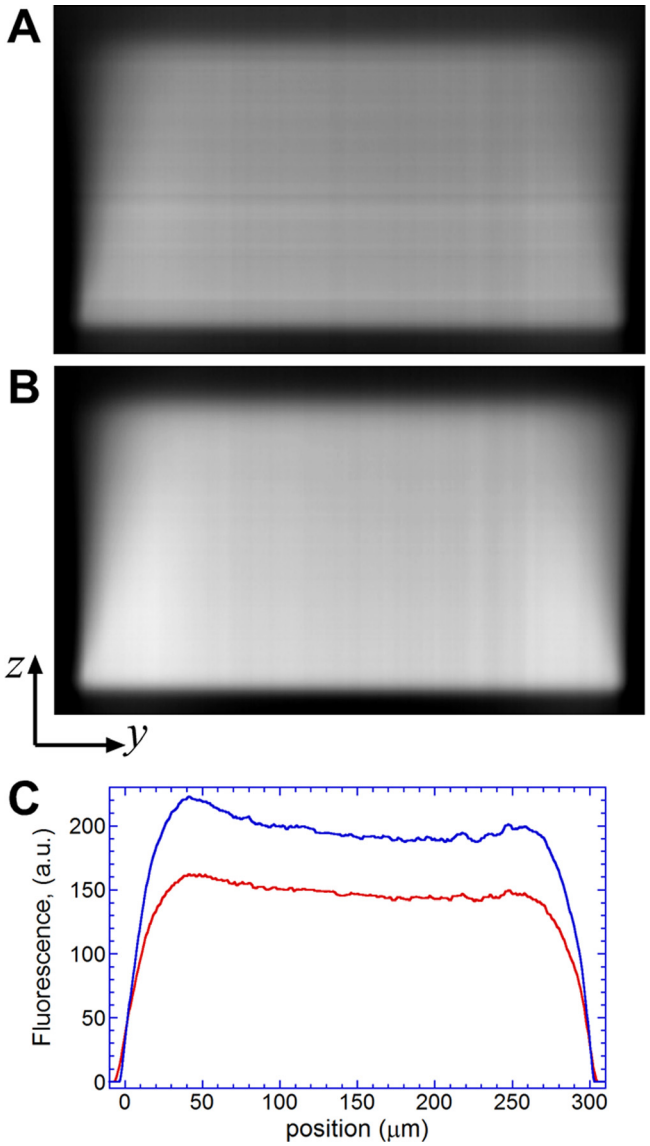

FIG. 2. Profiles of fluorescence in the *yz*-cross-section of the observation channel (300×180 μm in the *yz*-plane) of the microfluidic device reconstructed from confocal scans at different conditions. (a) Pressure at the buffer inlet is $P_{buf} = 5.0$ kPa, pressure at inlet 1 is $P_1 = 12$ kPa with a 10 ppm solution of fluorescein fed to it, and inlet 2 is blocked, resulting in 10 ppm fluorescein solution and buffer fed to mixer at ~3:1 ratio. (b) $P_1 = 12$ kPa, with the buffer inlet and inlet 1 blocked, resulting in pure 10 ppm fluorescein solution in the observation channel. (c) Profiles of fluorescence (in arbitrary units) along the *y*-axis taken at the channel mid-plane for the *yz*-cross-sections in panel a (red curve) and b (blue curve). Channel edges correspond to positions of 0 and 300 μm.

illumination intensity varying by <0.1% in a 20 min period.[42] We took fluorescence images of the observation channel near its central axis, ~200 μm from its entrance, and averaged the pixel values over an area ~25 μm in diameter to reduce the measurement error. For background correction, we took a fluorescence image of the same region without fluorescein in it, calculated the average pixel value of the region in this image and subtracted it from averaged pixel values in all other images. The solution fed to inlet 1 in this experiment had a fluorescein concentration $C_1^0 = 4$ ppm. From our previous calibration,[43] we expected the intensity of fluorescence in the 180 μm deep observation channel to be a linear function of fluorescein concentration, C_1, in the range from 0 to 4 ppm. Therefore, by measuring the fluorescence intensity and dividing

it by its value when the observation channel was flooded with the solution from inlet 1, we evaluated the fluorescein concentration normalized to its maximal value, $C^* = C_1/C_1^0$.

The dependence of C^* on $\Delta P_1 = P_1 - P_{th}$ was found to be a nearly perfect straight line in the entire range tested, from 0 to 5.2 kPa in ΔP_1 and from 0 to 0.56 in C^* (Fig. 3, black circles). (Higher values of ΔP_1 were not tested, because they required $P_1 > 10.5$ kPa that could not be generated hydrostatically with the existing setup, while the control of P_1 with compressed air provided ~20 times lower accuracy.) The root-mean-square of the differences between individual data points and a linear fit to the whole data set (21 points) was 0.0010, whereas the mean value of C^* was 0.287, indicating only ~0.35% average deviation of the values of C^* from the linear fit.

To test for possible dependence of C_1 on P_2, we repeated the experiment with inlet 2 unblocked and with $\Delta P_2 = P_2 - P_{th}$ set at 1 and 2 kPa (blue crosses and red plus signs in Fig. 3). These two values of ΔP_2 were expected to result, respectively, in ~10% and 20% of liquid in the mixer channel coming from inlet 2. This liquid that can be the stock solution of substance 2 was plain buffer in our case. The dependences of C^* on ΔP_1 with blocked inlet 2 and with ΔP_2 at 1 and 2 kPa were practically identical (Fig. 3), with slopes of 0.1062, 0.1060, and 0.1059, respectively, obtained from linear fits. (All 3 linear fits had $C^* = 0$ at $\Delta P_1 = -0.04$ kPa, most likely due to a 0.04 kPa error in the evaluation of P_{th}). Therefore, the experimental results showed no detectable dependence of C_1 on P_2, validating our analysis of the microchannel circuit and indicating that concentrations of substances from inlets 1 and 2 in the observation channel (C_1 and C_2) can be controlled and adjusted independently, by setting pressures at the respective inlets (P_1 and P_2).

D. Abrupt switching of concentration

We tested the response time of the mixer channel by connecting the syringe with 4 ppm fluorescein solution feeding inlet 1 to a source of pressurized air through a fast-acting solenoid valve with a low flow resistance (direct-acting P251SS-O12 by Ingersoll Rand with a ~7 ms switching time and a flow coefficient, $C_v = 0.69$). When the valve was off, the pressure at inlet 1 was $P_1 < P_{th}$ ($P_1 \approx 5.2$ kPa) and no fluorescein was fed to the mixer channel, resulting in $C_1 = 0$. When the valve was on, the pressure at inlet 1 was $P_1 > P_{th}$ ($P_1 \approx 10$ kPa) and the steady state concentration of fluorescein in the observation channel was $\sim 0.5\, C_1^0$. The valve was switched on and off with a period of ~4 s. The measurements of C_1 followed the same protocol as in the two previous experiments, with the difference that a Basler A102f digital camera was used, providing a sampling rate of 50 frames per second. The time dependence of

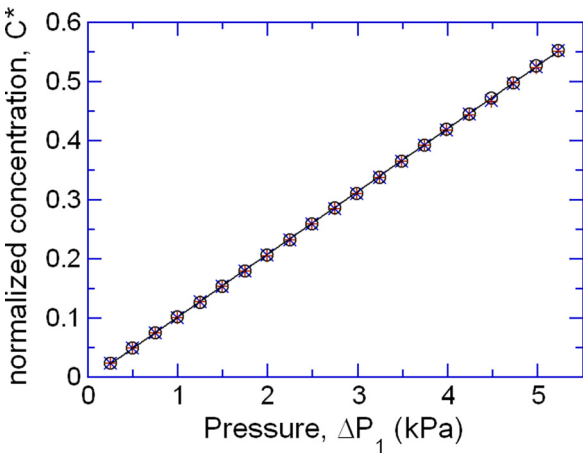

FIG. 3. Concentration of fluorescein in the observation channel normalized to fluorescein concentration in the stock solution, $C^* = C_1/C_1^0$, as a function of the level of pressure at inlet 1 above the threshold value, $\Delta P_1 = P_1 - P_{th}$, at different conditions: inlet 2 is blocked (black circles); buffer is fed to inlet 2 at $\Delta P_2 = P_2 - P_{th} = 1$ kPa (blue crosses); and buffer is fed to inlet 2 at $\Delta P_2 = 2$ kPa (red plus signs). The continuous line is a linear fit to the data points with inlet 2 blocked.

the normalized concentration (evaluated as fluorescence divided by its value at a steady state with the valve on) showed sharp transitions that occurred within $\Delta t \approx 250$ ms (based on the 10% to 90% criterion) for C_1 both increasing and decreasing [Fig. 4(a)]. To evaluate the delay between actuation of the valve and change in C_1, we used an LED producing a short pulse of light concurrently with the valve actuation and measured the interval between the pulse and the time point where C_1 was 50% through the transition. The interval was 0.79 s, which was very close to an estimate of the mean passage time through the mixer channel, $t = V_{mix}/Q_{mix} \approx 0.82$ s, as obtained using the total volume of the mixer channel, $V_{mix} = 0.22\ \mu$l, (22 segments with 0.010 μl volume each) and the volumetric flux through it, $Q_{mix} = 0.27\ \mu\text{l/s}$. The relation between the transition and passage times was $\Delta t \approx 0.31t$. (Within the 20 ms resolution of the camera, there was no delay between the actuation of the valve and the injection of the fluorescein solution into the mixer channel.) We also measured the mean concentration as a function of time during the periodic switching at various other points along the mixer channel, where the solution might not be completely mixed [Fig. 4(b)]. The switching time (based on the 10% to 90% criterion, again) varied as a square root of the distance from the mixer entrance, as counted by the number of mixing segments from the entrance, N, [Fig. 4(b)] the same as predicted by the Taylor-Aris theory[44,45] for rectilinear channel (see also Sec. IV). The dependence found from the best square root fit was $\Delta t = a\sqrt{N}$, with $a = 0.051$ s, corresponding to $\Delta t = bt^{0.5}$ with $b = 0.20\ \text{s}^{0.5}$.

E. Linear time ramps and waves of concentration

We initially tested the pneumatic setup for generation of linear ramps of pressure [Fig. 1(e)] by filling the 140 cc syringe with ~20 cc of water and connecting it to a long segment of transparent tubing with an internal diameter 0.5 mm (small enough to have minimal changes in the volume of air in the syringe, while large enough to have a low hydrodynamic resistance). The distal end of the capillary [Fig. 1(e)] was connected to a source of compressed air with a pressure $P_p = 40$ kPa. The transparent tubing was oriented vertically and placed in front of a ruler, and the height of the water column in the tubing was measured as a function of time after the 2-way valve was actuated, causing air flow through the capillary to raise pressure in the syringe. During ~100 s of observation, the water column height was observed to linearly increase in time (within ~3% experimental error), indicating a linear time ramp of pressure in the syringe.

We then filled the syringe with ~20 cc of 4 ppm solution of fluorescein in pH 7.5 phosphate buffer and connected it to inlet 1 of the microfluidic device. Inlet 2 was blocked and the

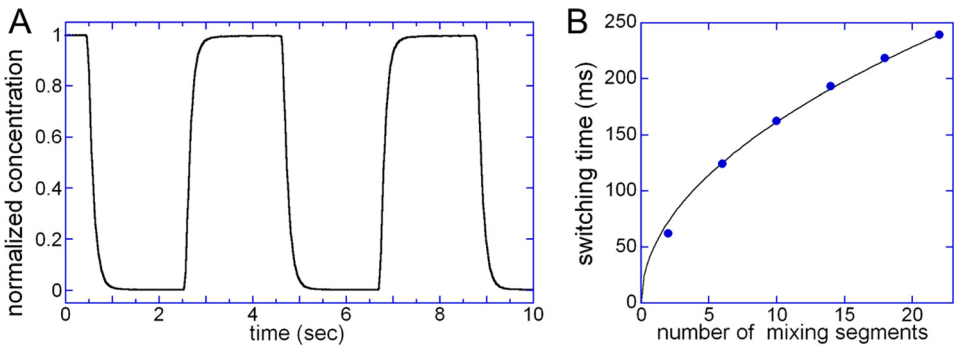

FIG. 4. Abrupt variation of fluorescein concentration by periodic switching of pressure at inlet 1 between ~5.2 kPa and ~10 kPa using a solenoid valve. (a) Time dependence of concentration of fluorescein in the observation channel normalized to its equilibrium value with the valve on, as measured by (background corrected) intensity of fluorescence using a digital camera operating at 50 frames per second. Transitions between 10% and 90% occur within ~0.25 s for both rising and falling concentration. (b) Switching time, Δt, defined as the transition time between 10% and 90% of the equilibrium level, at different positions along the mixer channel as a function of number of segments from the mixer entrance, N (blue circles). Continuous line is a fit to a square root dependence, $\Delta t \propto \sqrt{N}$.

buffer inlet was fed with plain buffer at $P_{buf} = 5.0$ kPa, as in the previous experiments. The pressure at inlet 1 was adjusted hydrostatically to a level just below P_{th}. The normalized concentration of fluorescein in the observation channel, $C^* = C_1/C_1^0$, was measured as a function of time, t, after the 2-way valve was actuated, while the capillary was connected to pressurized air with different P_p. The plots of C^* vs. t at $P_p = 20$, 40, 60, and 80 kPa [Fig. 5(a)] had several salient features. They were all smooth functions without appreciable fluctuations or irregularities. They were all well-fitted by functions $C^*(t) = A[1 - \exp(-t/\tau)]$ with the same time constant, τ, in agreement with our analysis. The value of τ was 3390 s, indicating that the growth of concentration with time remained linear within 1% for the first 34 s and within 5% for the first 170 s. The pressure-dependent pre-factors A that (together with τ) defined the initial slope of the time ramps had values of 1.37, 2.94, 4.77, and 6.68 at $P_p = 20$, 40, 60, and 80 kPa, respectively. The ratios of the pre-factors were 1:2.15:3.48:4.88, close to the ratios 1:2.18:3.54:5.09 predicted by the equation $dP_s/dt \approx (P_p^2 - P_{atm}^2)/(2R_cV)$, further validating our analysis of the setup operation. (The values of P_p entering this equation are absolute pressures equal to 120, 140, 160, and 180 kPa.)

As a final demonstration of capacities of the system, we used it to generate triangular concentration waves with different slopes on the falling side. To this end, the 3-way solenoid valve [Fig. 1(e)] had its normally open and normally closed ports connected to a source of pressurized air with $P_p = 60$ kPa and to a source of vacuum with variable negative gauge pressure, P_{vac}, respectively. The vacuum was first set at $P_{vac} = -80$ kPa and the valve was switched on and off for ~100 s during two ~200 s long cycles that generated a triangular wave of C_1 with nearly identical raising and falling slopes [equilateral triangles; Fig. 5(b), black lines]. After each 200 s cycle, the syringe was vented to the atmosphere [by briefly actuating the 2-way valve, Fig. 1(e)], resulting in an abrupt drop of C_1 to zero, so the second cycle was started from the same point as the first one. The value of P_{vac} was then changed to −40 kPa, resulting in a falling slope ~1.5 times smaller than the rising slope, and two periods of a different triangular wave were generated [blue lines in Fig. 5(b)]. Finally, a saw-tooth wave of concentration was generated with C^* raising to ~0.13 within 100 s and then abruptly falling to zero [red lines in Fig. 5(b)]. It was achieved by having the 3-way valve permanently on (the capillary connected to 60 kPa), while venting the syringe to the atmosphere every 100 s (by briefly actuating the 2-way valve).

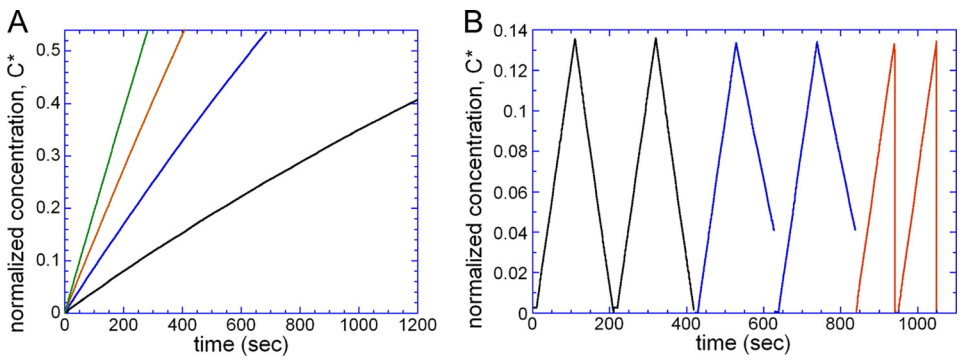

FIG. 5. Generation of linear time ramps and triangular waves of concentration using the microfluidic device and pneumatic setup with a capillary and syringe. (a) Normalized concentration of fluorescein in the observation channel, $C^* = C_1/C_1^0$, as a function of time after the 2-way valve is actuated sealing the syringe, while the distal end of the capillary is connected to compressed air with pressures, P_p, of 20 kPa (black line), 40 kPa (blue line), 60 kPa (red line), and 80 kPa (green line). (b) Various triangular waves of fluorescein concentration generated with the normally open port of the 3-way valve connected to compressed air with $P_p = 60$ kPa and with the valve switched at ~100 s intervals. Black lines: normally closed port of the 3-way valve is connected to vacuum at $P_{vac} = -80$ kPa; the 3-way valve is switched off at 0 at ~200 s and switched on at ~100 and ~320 s; the 2-way valve is briefly switched on at 0, ~200 s and ~420 s. Blue lines: normally closed port of the 3-way valve connected to vacuum at $P_{vac} = -40$ kPa; the 3-way valve is switched off at ~420 at ~630 s and on at ~530 and ~740 s; the 2-way valve is briefly switched on at ~420, ~630 s and ~840 s. Positive slopes are ~1.5 times steeper than negative slopes. Red lines: the 3-way valve is always on and the 2-way valve is briefly switched on at ~840, 940, and 1050 s, generating a saw-tooth wave of concentration.

IV. DISCUSSION

A. Performance of the setup

The proposed experimental system comprising the microfluidic device and the pressure ramp generating setup in Fig. 1 has several useful practical features. First, the system enables linear conversion of inlet pressure, P_1, into concentration of a substance in solution in an observation area, C_1, for C_1 ranging from zero all the way to the concentration of the stock solution fed to the inlet, C_1^0. The linear conversion is a consequence of the architecture of the microchannel network, with the mixer channel entrance connected through a negligible resistance channel to the buffer inlet and through high-resistance channels to the inlets 1 and 2. Second, the setup makes it possible to control concentrations of two substances independently by setting pressures at two inlets, with a linear conversion of pressures into respective concentrations and without any interdependence (cross-talk), as long as the sum of concentrations of the two substances (C_1 and C_2) normalized to their concentrations of the stock solutions (C_1^0 and C_2^0) is less than 1. (Independent control of concentrations of multiple substances was shown before with membrane pump metering.[37]) The microchannel network can be easily modified to enable independent variation of concentrations of 3 or more substances. Third, the switching of concentrations in a continuous range from 0 to C_1^0 occurs on a time scale of 0.25 s (based on the 10% to 90% criterion), which is expected to be shorter than the response time of most cells.[13–20] The switching time of 0.25 s is roughly equivalent to a maximal switching frequency of 2 Hz, about an order of magnitude higher than shown before.[17] Fourth, the system enables generation of smooth linear ramps of concentrations with a range of positive and negative slopes and triangular waves of concentration with various slopes. In the current system, the ramps remain linear (within 5%) over time scales $<$170 s, and the range of linearity can be readily extended if the time constant of the system, τ, is increased by augmenting the flow resistance of the capillary [smaller diameter or larger length; Fig. 1(e)]. We also note that the proposed microfluidic device could be used to rapidly switch concentration between a large number of discrete values, if the pressure at inlet 1 is derived from a specialized pneumatic setup, such as the 4-bit system based on solenoid valves with $\sim$25 ms pressure switching time.[46] Alternatively, electronically controlled pressure regulators or appropriately programmed motorized vertical stage could be used to generate concentration waves with harmonic profiles.

One of the advantages of the presented system as compared to previous microfluidic devices producing solutions with desired concentrations on demand and generating specific temporal profiles of concentration is the simplicity of the microchannel network. The network has a single channel layer and no integrated valves, and the control of concentration only requires a single source of regulated pressure that is linearly converted into concentration. In addition, the device operates continuously, with the flow velocity (and substrate shear stress) in the observation channel being defined by a constant pressure of the buffer inlet and remaining constant at varying concentrations. Therefore, cells on the substratum in the observation area are only presented with changes in concentration without concomitant changes in hydrodynamic stress.[26] In addition, the time ramps produced by the system are practically fluctuation-free.

B. Comparison of chaotic and laminar mixers

The combination of a relatively high volumetric flow rate, $Q_{mix} = 0.27\,\mu$l/s, short switching time, $\Delta t = 0.25$ s, and low driving pressure, $P_{buf} = 5$ kPa, is made possible by the mixer channel with chaotic 3D flow. It is instructive to compare this mixer with a laminar mixer, a narrow channel with a rectilinear flow, in which mixing occurs by diffusion only. Basic requirements to this laminar mixer are that it provides complete mixing, has short switching time, can handle sufficiently high volumetric fluxes, and operates at a reasonably low driving pressure.

An abrupt change in the ratio of flow rates of buffer and solution fed to the inlet of a laminar mixer would create a front propagating along the channel and spreading in the longitudinal direction. According to the Taylor-Aris theory,[44,45] for a round channel with a diameter d and mean flow velocity v, the spreading would occur with an effective diffusion coefficient

$$D_{eff} = D\left[1 + \frac{1}{192}\left(\frac{dv}{D}\right)^2\right] \approx \frac{1}{192}\frac{(dv)^2}{D}, \quad (1)$$

where $D = 500\ \mu m^2/s$ is the diffusion coefficient of fluorescein. The resulting width (longitudinal extension) of the front can then be estimated as

$$\Delta x = (2tD_{eff})^{1/2}, \quad (2)$$

where the mean time of passage through the channel, t, can be calculated as the quotient of the channel length, L, and v, $t = L/v$. The switching time, Δt, is the time it takes the diffusion-broadened front to pass through the mixer exit. Because the front has width Δx and moves with a mean flow velocity, v,

$$\Delta t = \Delta x/v = (2tD_{eff})^{1/2}/v = (2LD_{eff})^{1/2}/v^{3/2}. \quad (3)$$

Plugging in the expression for D_{eff} from Eq. (1) into Eq. (3), we obtain

$$\Delta t = [L(dv)^2/(96D)]^{1/2}/v^{3/2} = [Ld^2/(96Dv)]^{1/2}, \quad (4)$$

as equation relating the diameter of the channel, d, its length, L, coefficient of diffusion, D, the mean flow velocity, v, and the switching time, Δt. Its alternative form, using $t = L/v$, is

$$\Delta t = (t/96)^{1/2}(d^2/D)^{1/2}, \quad (5)$$

showing that Δt is proportional to the product of square roots of the passage time, t, and characteristic time of diffusive mixing across the channel, $t_{diff} = d^2/D$.

The condition for achieving good mixing by diffusion between two streams moving side by side through the channel is $t \geq t_{diff}$. If we set $t = t_{diff}$ for a minimal passage time, Eq. (5) becomes

$$\Delta t = t/\sqrt{96} \text{ or } \Delta t = t_{diff}/\sqrt{96} = d^2/(\sqrt{96}D), \quad (6)$$

indicating that, when t is set to a minimal value enabling good mixing, Δt is proportional to $t_{diff} = d^2/D$. Solving Eq. (6) for d and plugging in $D = 500\ \mu m^2/s$ and $\Delta t = 0.25$ s, we obtain $d = (96D^2\Delta t^2)^{1/4} \approx 35\ \mu m$ as the diameter of a laminar mixer channel providing the same switching time as our chaotic 3D mixer.

We now compare this laminar mixer with our 3D mixer in terms of the volumetric flux and driving pressure. A volumetric flux $Q_{mix} = 0.27\ \mu l/s$ corresponds to a mean flow velocity $v = 4Q_{mix}/(\pi d^2) = 0.28$ m/s through the 35 μm round channel, and the condition $t = t_{diff}$ requires a channel length $L = vt_{diff} = d^2v/D = 0.69$ m. According to the Poiseuille equation, for an aqueous solution with viscosity $\eta = 0.001$ Pa, these values of v and L would necessitate a driving pressure $P = 128vL\eta/(\pi d)^2 = 6.4 \cdot 10^6$ Pa or ~64 atm. This pressure is 3 orders of magnitude higher than $P_{buf} = 5$ kPa in our microfluidic system and would be practically impossible to achieve in a microfluidic device made of PDMS. If a pressure of 5 kPa is applied to a laminar mixer with $d = 35\ \mu m$, the conditions $t = t_{diff}$ (good mixing) and $\Delta t = 0.25$ s are met for a channel length $L \approx 19$ mm and $v \approx 7.8$ mm/s, corresponding to a volumetric flux of 0.0075 μl/s, which is ~36 times smaller than $Q_{mix} = 0.27\ \mu l/s$ achieved in our mixer. This greatly reduced volumetric flux would make the microfluidic device substantially less practical (e.g., by diminishing the region that can be exposed to the temporal wave of concentration with uncompromised time resolution). Therefore, the use of the chaotic 3D flow mixer rather than a diffusive laminar mixer in the microfluidic device was indeed essential, enabling large volumetric flux with a short switching time and low driving pressure.

We finally note that the length of a mixer channel required for a given quality of mixing, L, increases proportionally to the mean flow velocity, v, in the case of laminar mixers, but only as $v^{1/4}$ in the case of chaotic flow mixers.[2,47] As a result, the driving pressure, P, increases as v^2 for laminar mixers, but only as $v^{5/4}$ for chaotic mixers, making laminar mixers increasingly impractical when high flow rates are required. Furthermore, given the relation $L \propto v^{1/4}$ for chaotic mixers, the passage and switching times are expected to scale as $t = L/v \propto L^{-3}$ and $\Delta t \propto \sqrt{L}/v \propto L^{-7/2}$, respectively. This last expression suggests that the switching time can be substantially reduced (while maintaining a given quality of mixing) by increasing L. However, because $P \propto v^{5/4} \propto L^5$, leading to $P \propto \Delta t^{-10/7}$, the reduction of Δt would require increased driving pressure.

C. Prospective applications of the technique

The system presented here has been recently applied to study the response of social amoebas (*Dictyostelium discoideum*) to abrupt changes in concentration of chemoattractant (cyclic adenosine monophosphate).[26] Cellular responses were visualized with a fluorescent marker and were found to occur on a 1–10 s scale, which was well within the range of time resolution of the proposed system.[26] The system can also be applied to other chemotactic eukaryotic cells, such as primary neutrophils and HL60 neutrophil-like cells, where the elucidation of temporal response to specific stimuli can help better understand the workings of chemotactic signaling pathways, and find multiple additional applications in cell biology. In particular, it can enable repeating the classic experiments on exposure of chemotactic *E. coli* to time ramps of concentration of chemoattractant[14] in a microfluidic format with a reduced level of fluctuations and high linearity of the ramps, potentially enabling finding the limits of sensitivity and adaptation (a rate of concentration variation that does not elicit a detectable response).[14] Moreover, because the proposed system allows independent variation of concentrations of two substances, it can be used to challenge cells with conflicting external signals, such as an increase of concentration of one attractant with simultaneous reduction of concentration of another (or increase of concentration of a repellent).[48,49] Responses of cells to stimuli of this type with varying strength of the two signals may provide valuable information about cellular signal processing. More broadly, the temporal ramps of concentration in a microfluidic device of the type presented here can help study the signaling dynamics or behavior of any cell[21,22] or a small model organism (e.g., *Caenorhabditis elegans* worm[50]) that responds to the chemical content of the medium on a 1–100 s time scale.

The capacity to accurately control multiple concentrations by varying pressures and to apply slow time ramps could also prove useful for studies of concentration dependence of conformations and states of assembly of bio-molecular complexes (proteins, nucleic acids, and their aggregates) on the substratum in the observation channel using total internal reflection fluorescence (TIRF) microscopy.[51–53] The observable could be the intensity of fluorescence or efficiency of Förster resonance energy transfer (FRET), which are well suited for microfluidic experiments.[54–56] Specifically, variation of concentrations of two (or more) reagents can help obtaining two- (or multi-) dimensional biochemical phase diagrams of the type previously obtained with spatial two-dimensional gradients.[54] As it has been recently shown with a membrane valve based microfluidic system,[56] coordinated variation of concentrations by steps and continuous ramps could also be particularly suitable for single-molecule spectroscopy in solution using confocal microscopy, where the analysis is normally limited to a single point in space.

ACKNOWLEDGMENTS

We thank Michael Erickstad for his help with the experiments. The work was partly funded by NIH Grant Nos. P01 GM078586 and R01 GM084332.

[1]A. D. Stroock, S. K. Dertinger, A. Ajdari *et al.*, Science **295**, 647 (2002).
[2]C. Simonnet and A. Groisman, Phys. Rev. Lett. **94**, 134501 (2005).
[3]M. A. Unger, H. P. Chou, T. Thorsen *et al.*, Science **288**, 113 (2000).

[4]C. L. Hansen, E. Skordalakes, J. M. Berger *et al*., Proc. Natl. Acad. Sci. U.S.A. **99**, 16531 (2002).
[5]N. L. Jeon, S. K. W. Dertinger, D. T. Chiu *et al*., Langmuir **16**, 8311 (2000).
[6]S. K. W. Dertinger, D. T. Chiu, N. L. Jeon *et al*., Anal. Chem. **73**, 1240 (2001).
[7]N. L. Jeon, H. Baskaran, S. K. W. Dertinger *et al*., Nat. Biotechnol. **20**, 826 (2002).
[8]R. Ferrigno, J. N. Lee, X. Y. Jiang *et al*., Anal. Chem. **76**, 2273 (2004).
[9]D. M. Thompson, K. R. King, K. J. Wieder *et al*., Anal. Chem. **76**, 4098 (2004).
[10]P. J. Hung, P. J. Lee, P. Sabounchi *et al*., Biotechnol. Bioeng. **89**, 1 (2005).
[11]J. Pihl, J. Sinclair, E. Sahlin *et al*., Anal. Chem. **77**, 3897 (2005).
[12]U. Levy, K. Campbell, A. Groisman *et al*., Appl. Phys. Lett. **88**, 111107 (2006).
[13]S. M. Block, J. E. Segall, and H. C. Berg, Cell **31**, 215 (1982).
[14]S. M. Block, J. E. Segall, and H. C. Berg, J. Bacteriol. **154**, 312 (1983).
[15]J. E. Segall, S. M. Block, and H. C. Berg, Proc. Natl. Acad. Sci. U.S.A. **83**, 8987 (1986).
[16]A. Groisman, C. Lobo, H. Cho *et al*., Nat. Methods **2**, 685 (2005).
[17]M. R. Bennett, W. L. Pang, N. A. Ostroff *et al*., Nature (London) **454**, 1119 (2008).
[18]G. Charvin, F. R. Cross, and E. D. Siggia, PLoS ONE **3**, e1468 (2008).
[19]K. R. King, S. Wang, A. Jayaraman *et al*., Lab Chip **8**, 107 (2008).
[20]D. Irimia, Annu. Rev. Biomed. Eng. **12**, 259 (2010).
[21]P. Hersen, M. N. McClean, L. Mahadevan *et al*., Proc. Natl. Acad. Sci. U.S.A. **105**, 7165 (2008).
[22]J. T. Mettetal, D. Muzzey, C. Gomez-Uribe *et al*., Science **319**, 482 (2008).
[23]E. Albrecht and H. R. Petty, Proc. Natl. Acad. Sci. U.S.A. **95**, 5039 (1998).
[24]J. Geiger, D. Wessels, and D. R. Soll, Cell Motil. Cytoskeleton **56**, 27 (2003).
[25]M. Etzrodt, H. C. F. Ishikawa, J. Dalous *et al*., FEBS Lett. **580**, 6707 (2006).
[26]K. Takeda, D. Shao, M. Adler *et al*., Science Signaling **5**, ra2 (2012).
[27]A. Jovic, B. Howell, M. Cote *et al*., PLOS Comput. Biol. **6**, e1001040 (2011).
[28]A. Jovic, S. M. Wade, A. Miyawaki *et al*., Mol. Biosyst. **7**, 2238 (2011).
[29]P. Sabounchi, C. Ionescu-Zanetti, R. Chen *et al*., Appl. Phys. Lett. **88**, 183901 (2006).
[30]J. Sun, J. Wang, P. Chen *et al*., Anal. Bioanal. Chem. **400**, 2973 (2011).
[31]J. Olofsson, H. Bridle, J. Sinclair *et al*., Proc. Natl. Acad. Sci. U.S.A. **102**, 8097 (2005).
[32]E. Eriksson, K. Sott, F. Lundqvist *et al*., Lab Chip **10**, 617 (2010).
[33]P. J. Lee, T. A. Gaige, and P. J. Hung, Lab Chip **9**, 164 (2009).
[34]G. A. Cooksey, C. G. Sip, and A. Folch, Lab Chip **9**, 417 (2009).
[35]L. Chen, F. Azizi, and C. H. Mastrangelo, Lab Chip **7**, 850 (2007).
[36]F. Azizi and C. H. Mastrangelo, Lab Chip **8**, 907 (2008).
[37]A. Ainla, I. Gozen, O. Orwar *et al*., Anal. Chem. **81**, 5549 (2009).
[38]X. Y. Zhang and M. G. Roper, Anal. Chem. **81**, 1162 (2009).
[39]L. R. Cao, X. Y. Zhang, A. Grimley *et al*., Anal. Bioanal. Chem. **398**, 1985 (2010).
[40]A. Groisman, M. Enzelberger, and S. R. Quake, Science **300**, 955 (2003).
[41]H. L. Dryden, F. D. Murnaghan, and H. Bateman, *Hydrodynamics* (Dover, New York, 1956).
[42]M. Polinkovsky, E. Gutierrez, A. Levchenko *et al*., Lab Chip **9**, 1073 (2009).
[43]K. Campbell and A. Groisman, Lab Chip **7**, 264 (2007).
[44]G. Taylor, Proc. R. Soc. London **219**, 186 (1953).
[45]R. Aris, Proc. R. Soc. London **235**, 67 (1956).
[46]K. Campbell, Y. Fainman, and A. Groisman, Appl. Phys. Lett. **91**, 171111 (2007).
[47]T. Burghelea, E. Segre, and V. Steinberg, Phys. Rev. Lett. **92**, 164501 (2004).
[48]M. Kim and T. Kim, Anal. Chem. **82**, 9401 (2010).
[49]Y. Kalinin, S. Neumann, V. Sourjik *et al*., J. Bacteriol. **192**, 1796 (2010).
[50]S. H. Chalasani, N. Chronis, M. Tsunozaki *et al*., Nature (London) **450**, 63 (2007).
[51]C. W. Hollars, J. Puls, O. Bakajin *et al*., Anal. Bioanal. Chem. **385**, 1384 (2006).
[52]D. L. Chen, W. B. Du, and R. F. Ismagilov, New J. Phys. **11** (2009).
[53]B. R. Schudel, M. Tanyeri, A. Mukherjee *et al*., Lab Chip **11**, 1916 (2011).
[54]V. Vandelinder, A. C. M. Ferreon, Y. Gambin *et al*., Anal. Chem. **81**, 6929 (2009).
[55]E. A. Lemke, Y. Gambin, V. Vandelinder *et al*., J. Am. Chem. Soc. **131**, 13610 (2009).
[56]S. Kim, A. M. Streets, R. R. Lin *et al*., Nat. Methods **8**, 242 (2011).